Simultaneous Realization of Phase/Size Manipulation, Upconversion Luminescence Enhancement, and Blood Vessel Imaging in Multifunctional Nanoprobes Through Transition Metal Mn^{2+} Doping

Songjun Zeng, Zhigao Yi, Wei Lu, Chao Qian, Haibo Wang, Ling Rao, Tianmei Zeng, Hongrong Liu,* Huijing Liu, Bin Fei, and Jianhua Hao**

A strategy is demonstrated for simultaneous phase/size manipulation, multicolor tuning, and remarkably enhanced upconversion luminescence (UCL), particularly in red emission bands in fixed formulae of general lanthanide-doped upconverting nanoparticles (UCNPs), namely $NaLnF_4$:Yb/Er (Ln: Lu, Gd, Yb), simply through transition metal Mn^{2+}-doping. The addition of different Mn^{2+} dopant contents in $NaLnF_4$:Yb/Er system favors the crystal structure changing from hexagonal (β) phase to cubic (α) phase, and the crystal size of UCNPs can be effectively controlled. Moreover, the UCL can be tuned from green through yellow and to dominant red emissions under the excitation of 980 nm laser. Interestingly, a large enhancement in overall UCL spectra of Mn^{2+} doped UCNPs (~59.1 times for $NaLuF_4$ host, ~39.3 times for $NaYbF_4$ host compared to the UCNPs without Mn^{2+} doping) is observed, mainly due to remarkably enhanced luminescence in the red band. The obtained result greatly benefits in vitro and in vivo upconversion bioimaging with highly sensitive and deeper tissue penetration. To prove the application, a select sample of nanocrystal is used as an optical probe for in vitro cell and in vivo bioimaging to verify the merits of high contrast, deeper tissue penetration, and the absence of autofluorescence. Furthermore, the blood vessel of lung of a nude mouse with the injection of Mn^{2+}-doped $NaLuF_4$: Yb/Er UCNPs can be readily visualized using X-ray imaging. Therefore, the Mn^{2+} doping method provides a new strategy for phase/size control, multicolor tuning, and remarkable enhancement of UCL dominated by red emission, which will impact on the field of bioimaging based on UCNP nanoprobes.

1. Introduction

Lanthanide doped UCNPs are well known for their biological applications because of their unique energy UCL capabilities, resulting from the effective absorption of low-energy photons followed by emitting high-energy photons.[1–39] The red region (600–700 nm) and near-infrared (NIR) spectral range (700–1100 nm) are generally addressed as the "optical window" of the biological tissues, due to the lack of efficient endogenous absorbers.[40,41] Therefore, bringing the excitation and emission peaks into the "optical window" is of significant importance for in vivo optical bioimaging with deeper tissue penetration. Yb/Er co-doped $NaLnF_4$ (Ln = Y, La, Lu, Yb, Gd) hosts are considered as the most efficient UCL systems. However, most of these UCNPs[18,23,26] such as $NaYF_4$, $NaLuF_4$, $NaGdF_4$ doped with Yb/Er usually present intense green UCL, which hinders their application in in vivo bioimaging for deeper tissue penetration owing to the intense tissue absorption of short wavelengths light

Prof. S. J. Zeng, C. Qian, T. M. Zeng, Prof. H. R. Liu
College of Physics and Information Science
and Key Laboratory of Low-dimensional Quantum Structures
and Quantum Control of the Ministry of Education
Hunan Normal University
Changsha 410081, China
E-mail: songjunz@hunnu.edu.cn; hrliu@hunnu.edu.cn

Z. G. Yi, H. B. Wang, L. Rao
Faculty of Materials
Optoelectronics and Physics
Key Laboratory of Low-dimensional Materials
and Application Technology (Ministry of Education)
Xiangtan University
Xiangtan 411105, PR China

Dr. W. Lu, Prof. J. H. Hao
Department of Applied Physics
and Materials Research Center
The Hong Kong Polytechnic University
Hong Kong, China
E-mail: jh.hao@polyu.edu.hk

Dr. H. J. Liu
CAS Key Laboratory of Brain Function and Disease
the Center for Integrative Imaging (CII) of
Hefei National Laboratory for Physical Science at the Microscale
and Department of Neurobiology and Biophysics School of Life Sciences
University of Science and Technology of China
Hefei 230027, China

Prof. B. Fei
Institute of Textiles & Clothing
The Hong Kong Polytechnic University
Hong Kong, China

DOI: 10.1002/adfm.201304270

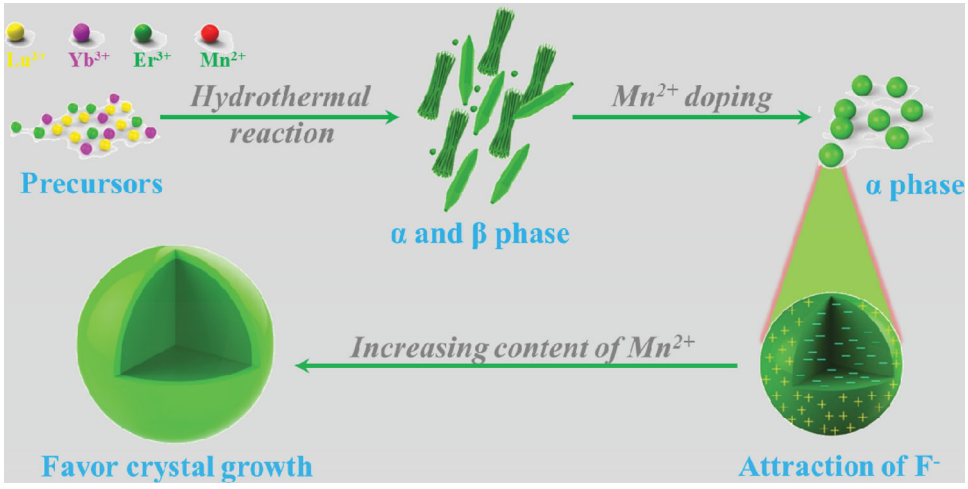

Scheme 1. Schematic illustration of the phase, size and morphology evolution mechanism of $NaLuF_4$:Mn/Yb/Er UCNPs via increasing the content of Mn^{2+}.

(<600 nm).[40,41] In addition, it is still a challenge to achieve multi-color output and enhanced red UCL in a single fixed composition of Yb/Er co-doped system.

In addition to the wavelength of emission, another consideration is the brightness of UCNPs for bioimaging.[42] Generally speaking, the brighter the nanoprobes means the higher signal-to-noise ratio which may be achieved in bioimaging system. Unfortunately, one of main drawbacks for UCL materials is their quite low quantum efficiency,[34] although some approaches, such as our proposed electric-field,[43] increase in doping concentration recently reported by Zhao et al.[39] On the other hand, size, shape and phase of UCNPs have also great influence on their luminescence and biological application. Thus, as ideal UCNPs based bioprobes, all these properties should be fully considered. However, simultaneous control of structure (nanocrystal size, shape, and phase) and enhancement in UCL, especially dominated by red emission in UCNPs with fixed formula is still a great challenge and rarely reported. A few reports have been related to the enhancement in red emission, such as Yb/Er co-doped $KMnF_3$ by Liu's group,[40] and Mn^{2+} doped $NaYF_4$:Yb/Er.[41] In the reported UCNPs systems, red-to-green (R/G) ratio can be greatly enhanced owing to the energy transfer between Mn^{2+} and Er^{3+}.

In this work, we propose a strategy to simultaneously realize phase/size control, multi-color output and enhanced UCL in general lanthanides doped UCNPs, i.e. Yb/Er co-doped $NaLnF_4$ systems with fixed composition via tuning single transition metal ion (Mn^{2+}) instead of the change in the composition of lanthanide ions (Yb^{3+} and Er^{3+}). $NaLnF_4$ (Ln = Lu, Gd, Yb) hosts also show larger X-ray absorption[30,44–46] property compared to Y-based host. We adopted a modified facile hydrothermal method[7,41,47] to synthesize the Mn^{2+} doped $NaLnF_4$ UCNPs. In vitro/in vivo upconversion fluorescent bioimaging and *in vivo* X-ray imaging based on the developed UCNPs have been demonstrated to validate the ability of these UCNPs for bioimaging. Interestingly, significant signal of blood vessel of lung can be observed, which is essential to improve the detection of the lung and pulmonary vascular diseases.

2. Results and Discussion

2.1. Doping Induced Phase/Size Control

As shown in the schematic diagram (**Scheme 1**), the phase transformation, size change and morphology evolution of $NaLuF_4$:Mn/Yb/Er UCNPs can be realized via Mn^{2+} doping. **Figure 1** shows X-ray diffraction patterns (XRD) of the as-prepared $NaLuF_4$: Mn/Yb/Er (x/18/2 mol%). The majority of β phase and minor α phase of $NaLuF_4$:Yb/Er are presented while absence of Mn^{2+}. Furthermore, the phase transformation from the coexistence of α- and β-phases to pure α-phase is completed through increasing Mn^{2+} content, and pure α-phase can be obtained when the Mn^{2+} content reaches up to 5%. No other diffraction peaks were observed even Mn^{2+} content was increased up to 40%. In addition, the diffraction peak shifts slightly towards higher angle side as a function of Mn^{2+} content. This is mainly attributed to the decrease in unit-cell volume of

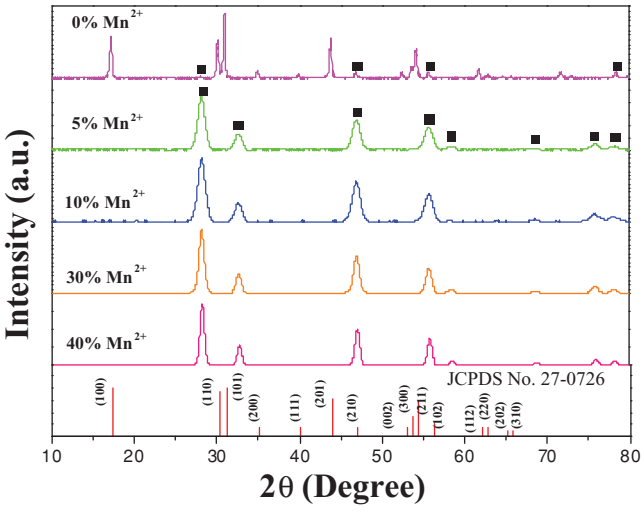

Figure 1. X-ray diffraction patterns of $NaLuF_4$:Mn/Yb/Er (x/18/2 mol%) by doping different Mn^{2+} contents at 0, 5, 10, 30, and 40 mol%. The diffraction peaks of α-phase were marked by black rectangular labels.

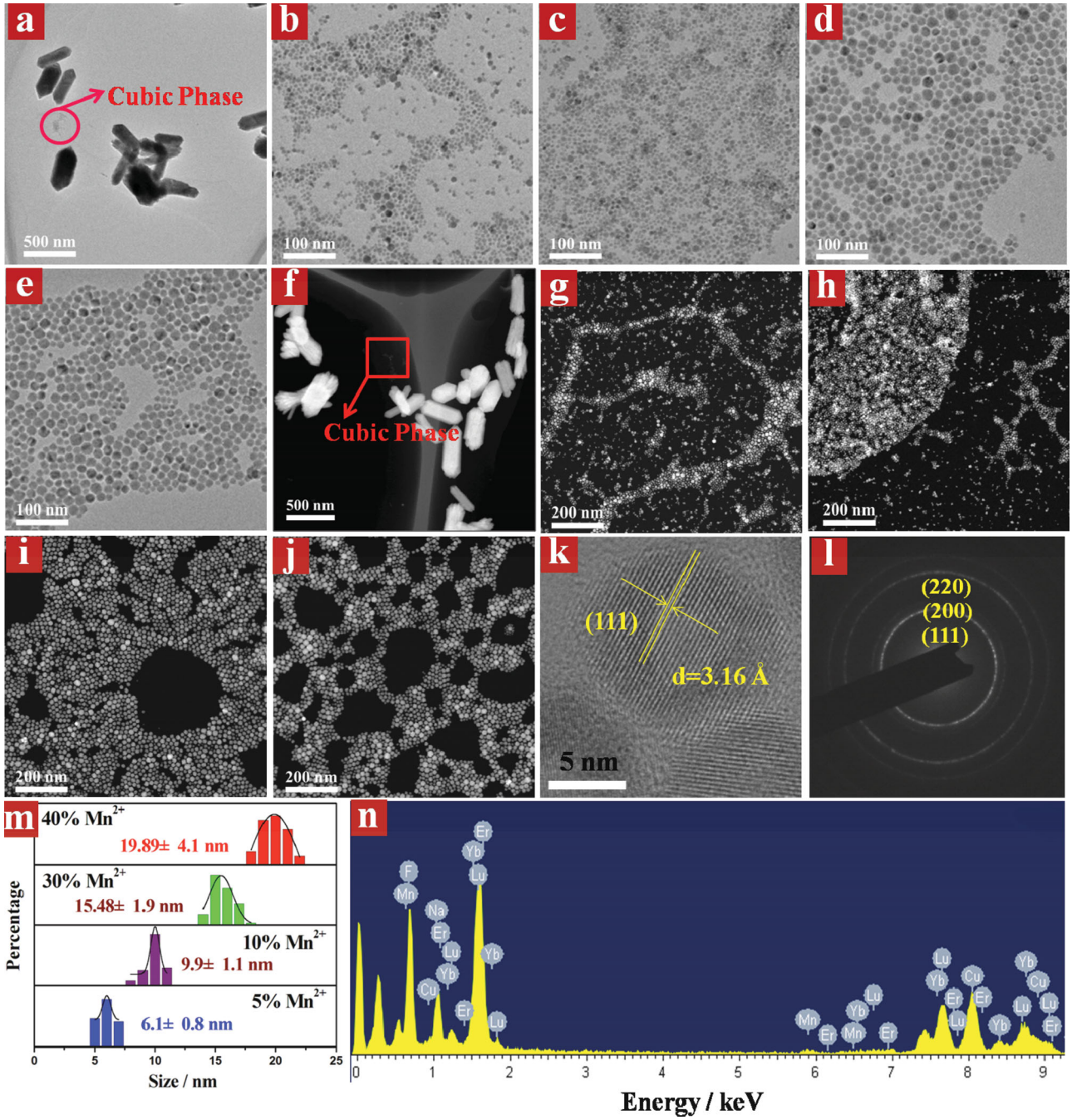

Figure 2. (a–e) Typical TEM images of $NaLuF_4$:Mn/Yb/Er UCNPs doped with different Mn^{2+} contents (0, 5, 10, 30, and 40%), respectively, (f–j) the STEM images of the corresponding $NaLuF_4$ UCNPs shown in (a–e), respectively. The α-phase UCNPs are marked by red closed lines in (a) and (f). (k) HRTEM image taken from single particle in (e), (l) SAED taken from (e) and (n) EDS of the as-prepared UCNPs shown in (e), (m) the size distribution of $NaLuF_4$ host for the increased Mn^{2+} contents. Scale bars are 500 nm for panels (a) and (f), 100 nm for panels (b–e) and (g–j), and 5 nm for panel (k).

$NaLuF_4$ host owing to the replacement of Lu^{3+} ion (r = 1.117 Å) by Mn^{2+} with relatively smaller radius (r = 1.10 Å).[48] During the phase transformation, the size of the as-prepared UCNPs increases simultaneously as an evidence of gradually narrowed diffraction peaks by increasing Mn^{2+} content.

To further reveal the phase and size control, we performed transmission electron microscopy (TEM) and scanning transmission electron microscopy (STEM) analyses. Without doping of Mn^{2+}, the sample is composed of hexagonal microrods and besom-like microsticks (β-phase) and small cubic nanosphere (α-phase) by TEM and STEM images (**Figure 2**a,f). When adding Mn^{2+}, as demonstrated in Figure 2b–e,g–j, high-quality uniform nanospheres of $NaLuF_4$:Mn/Yb/Er UCNPs with pure α-phase can be obtained, and their size is changed from 6.1 nm to 19.9 nm (Figure 2m) by varying the content of Mn^{2+} from 5% to 40%. High resolution TEM (HRTEM) image

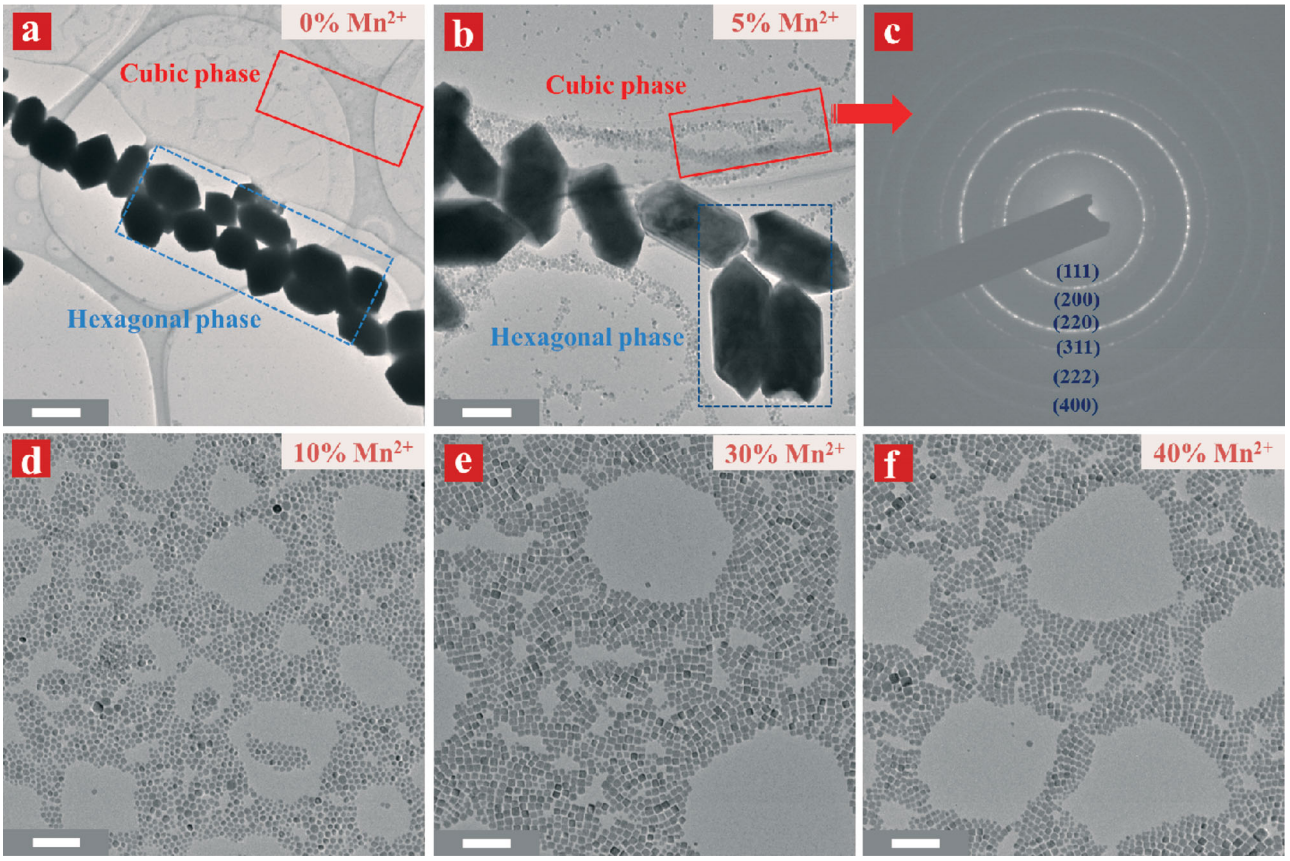

Figure 3. (a,b,d–f) Typical TEM images of $NaYbF_4$:Mn/Er UCNPs doped with different Mn^{2+} contents (0, 5, 10, 30, and 40%), respectively. The full red and dotted green rectangles presented in (a) and (b) show the cubic and hexagonal phase of the corresponding UCNPs, respectively. (c) The SAED analysis of UCNPs taken from (b), indicating the face-centered cubic structure. Scale bars are 1 μm for (a), 200 nm for (b), and 100 nm for (d–f).

(Figure 2k) of a single particle taken from Figure 2e shows the measured interplanar spacing of 3.16 Å, matching well with the (111) crystal plane of α-phase. Figure 2l shows the typical selected area electron diffraction (SAED) of UCNPs taken from Figure 2e, in which the formation of pure α-phase structure is evident. Moreover, energy dispersive X-ray spectrometer (EDS) analysis (Figure 2n) taken from Figure 2e shows the presence of Na, Lu, F, and doped Yb, Mn, Er elements, further verifying the substitution of Lu^{3+} by Mn^{2+}. These results demonstrate that the phase, shape, and size of $NaLuF_4$ UCNPs can be readily tuned by adjusting the doped Mn^{2+} contents. The phase transformation from β- to α-phase could be mainly ascribed to the substitution of large sized Lu^{3+} (r = 1.117 Å)[48] by relative smaller sized Mn^{2+} (r = 1.10 Å),[48] which is consistent with the previous reports (the smaller substitution ions tend to produce the cubic phase).[8,41] Meanwhile, the substitution of Lu^{3+} by Mn^{2+} may generate positive vacancies on the grain surface for the charge balance, subsequently forming transient electric dipoles with the positive poles pointing outward[49] (as shown in Scheme 1), which can greatly accelerate the diffusion of F ions from the solution to the grain, and therefore promote the growth of $NaLuF_4$ UCNPs with increasing Mn^{2+} content.

To shed more light on the influence of Mn^{2+} doping in $NaLnF_4$ host, we synthesized some other UCNPs, such as $NaGdF_4$ and $NaYbF_4$ by the same method. As shown in Figure S1, obvious phase transformation from β to α induced by Mn doping is observed in $NaYbF_4$ host, when the Mn^{2+} content ranges from 5% to 10%. To further reveal the phase/size control, TEM analysis was performed in Mn^{2+} doped $NaYbF_4$ host. As demonstrated in **Figure 3**, Mn-free and 5% Mn^{2+} doped samples possess two types of structures such as large scale β-phase particle and small sized α-phase nanocrystals. When further increasing the content of Mn^{2+}, all of the β-phase particles were transformed to small sized α-phase nanocrystals, indicating the simultaneous phase/size control in $NaYbF_4$ host via Mn^{2+} doping. Moreover, XRD (Figure S2) and TEM (Figure S3) analyses of Mn^{2+} doped $NaGdF_4$ UCNPs also indicate the obvious phase transformation from β- to α-phase and size/morphology evolution. Therefore, the Mn^{2+} doping method can be extended to the other $NaLnF_4$ systems for simultaneous phase/size control.

2.2. Remarkable Enhancement of Red Upconversion Emission and Tunable Multi-Color Output

Intense red UCL is beneficial for in vivo bioimaging owing to the low tissue absorption.[40] However, it is still a great challenge to realize multi-color emissions and enhance UCL particularly red emission band in a fixed composition of Yb/Er doped system. **Figure 4**b shows the upconversion spectra of Mn^{2+} doped

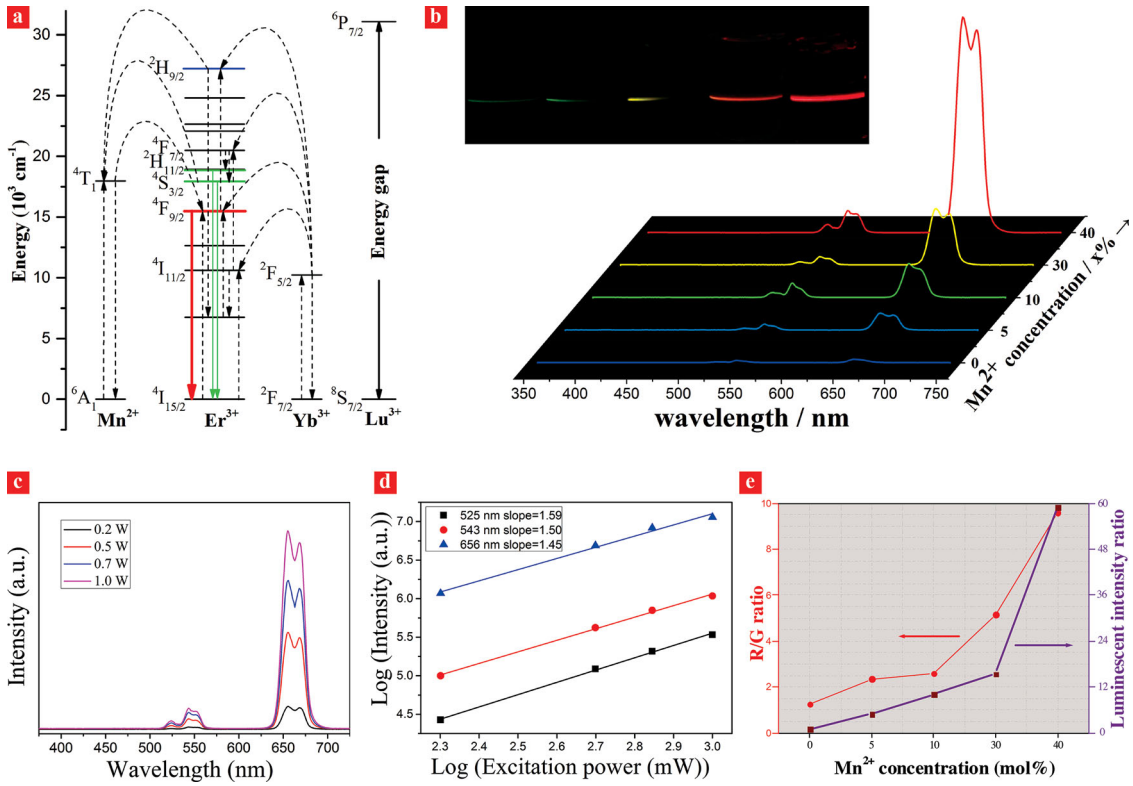

Figure 4. UCL studies of $NaLuF_4$:Mn/Yb/Er (x/18/2 mol%) UCNPs. (a) Proposed energy transfer mechanisms under the excitation of 980 nm laser, (b) UCL spectra of the as-synthesized UCNPs doped with different content of Mn^{2+}, (c) power dependent UCL spectra, (d) the corresponding Log (upconversion intensity)–Log (excitation power) plots, (e) the calculated R/G ratio (red curve) and the whole UCL intensity (purple curve). The insets of b show the corresponding digital photographs of cyclohexane solutions containing 1 wt% UCNPs doped with 0, 5, 10, 30, and 40% Mn^{2+}, respectively, under the excitation of 980 nm with power density of 1 W cm^{-2}.

$NaLuF_4$:Yb/Er UCNPs. As demonstrated, the whole UCL intensity was gradually enhanced by increasing Mn^{2+} content. And compared with the Mn-free sample, the whole UCL intensity has been significantly enhanced by 59.1 times (Figure 4e). The digital photographs (insets of Figure 4b) show obvious multicolor tuning from green through yellow and finally to red. It is apparent that the brightness of light is also significantly enhanced by naked eyes, which is consistent with the UCL spectra. Moreover, with increasing the Mn^{2+} content, the remarkably enhanced red UCL was achieved and the R/G ratio was increased from 1.2 to 9.6 (Figure 4e). To further investigate Mn^{2+} doping on the effect of UCL property of $NaLuF_4$ host, a proposed energy transfer mechanism of Mn/Yb/Er triply-doped $NaLuF_4$ system is analyzed here. As presented in Figure 4a, the intense red UCL can be ascribed to non-radiative energy transfer from the Er^{3+} to Mn^{2+} ($^2H_{9/2}/^4S_{3/2} \rightarrow ^4T_1$), followed by back-energy transfer to Er^{3+} ($^4T_1 \rightarrow ^4F_{9/2}$).[40,41] With increasing the content of Mn^{2+}, the barely changed weak green and greatly enhanced red emissions of Er^{3+} indicate extremely efficient inter-energy transfer between Er^{3+} and Mn^{2+}. As a result, higher R/G ratio can be achieved. To further study the photon excitation process, power dependent UCL spectra of $NaLuF_4$:Mn/Yb/Er (40/18/2 mol%) were performed. As shown in Figure 4c,d, the slopes of UCL in the wavelength of 525, 543, and 656 nm are 1.59, 1.50, and 1.45, respectively, indicating that the weak green and dominant red UCL of Er^{3+} are both ascribed to two photons processes.

Besides, the UCL spectra (Figure S4) and the digital photographs (insets of Figure S4) also reveal that the tunable multicolor output from green to red and enhanced red UCL can be successfully achieved by adjusting Mn^{2+} content in $NaGdF_4$ host. While in $NaYbF_4$:Mn/Yb/Er system, single-band red UCL of these UCNPs can be obtained and the whole UCL intensity is enhanced by 39.3 times (Figure S5) compared to the Mn-free sample. In $NaYbF_4$ host, the dominant red UC emission in $NaYbF_4$:Er UCNPs may be attributed to the cross-relaxation process ($^4F_{7/2} \rightarrow ^4F_{9/2}$, $^4F_{9/2} \leftarrow ^4I_{11/2}$) of Er^{3+}.[50,51] The higher Yb^{3+} concentration makes more efficient cross-relaxation process occurred and subsequently enhances the electron population in $^4F_{9/2}$ level of Er^{3+}, which is consistent with our previous report.[51] Therefore, the Mn^{2+} doping can not only realize multi-color output and significantly enhance red UCL, but also improve the overall UCL intensity. Such an enhancement in overall UCL intensity may attribute to the change in surrounding environment of light-emitting rare-earth ions and the efficient cross-relaxation of energy between Er and Mn ions.[40,41]

2.3. In Vitro Cell Imaging

To further study the in vitro and in vivo bioimaging properties of these Mn^{2+}-doped $NaLnF_4$ systems, $NaLuF_4$:Mn/Yb/Er

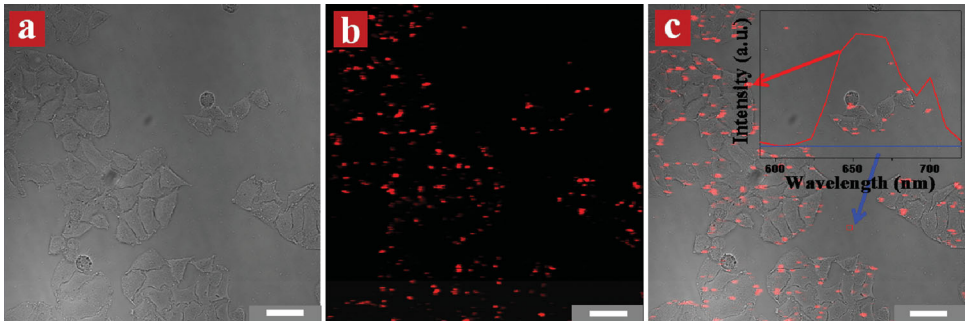

Figure 5. In vitro bioimaging of HeLa cells treated with $NaLuF_4$:Mn/Yb/Er UCNPs. (a) Bright field image of HeLa cells, (b) fluorescent image (λex = 980 nm, emission filter range: 600–700 nm), (c) overlay image, and the inset of which shows the localized UCL spectra taken from HeLa cells and background. Scale bars are 50 μm for all images.

(40/18/2 mol%) UCNPs have been selected and converted to water solubility by treating with HCl[32] for bioimaging. The dominant red UCL and overall intense UCL from $NaLuF_4$:Mn/Yb/Er make it ideal probe for in vitro and in vivo bioimaging with high contrast and deep penetration depth. **Figure 5** presents in vitro bioimaging of HeLa cells treated with these UCNPs (100 μg mL^{-1}) in an atmosphere of 5% CO_2 for 4 h at 37 °C.[52] The luminescent signals of UCNPs with emission spectra (600–700 nm) were detected, and bright red UCL can be obtained (Figure 5b), indicating the internalization of UCNPs in HeLa cells. Figure 5c shows the overlay image, verifying that the UCL signal is from the HeLa cells. Moreover, the localized UCL spectra taken from HeLa cells and background further reveal that the red signal exhibits the UCL with high contrast and absence of auto-fluorescence, making $NaLuF_4$:Mn/Yb/Er UCNPs ideal probes for in vitro bioimaging with high signal-to-noise ratio and sensitivity. Figure S6 shows the pumping power dependent bioimaging of HeLa cells. As illustrated, with increasing the power, the UCL signal is gradually enhanced and the UCL signal can be detected at low power.

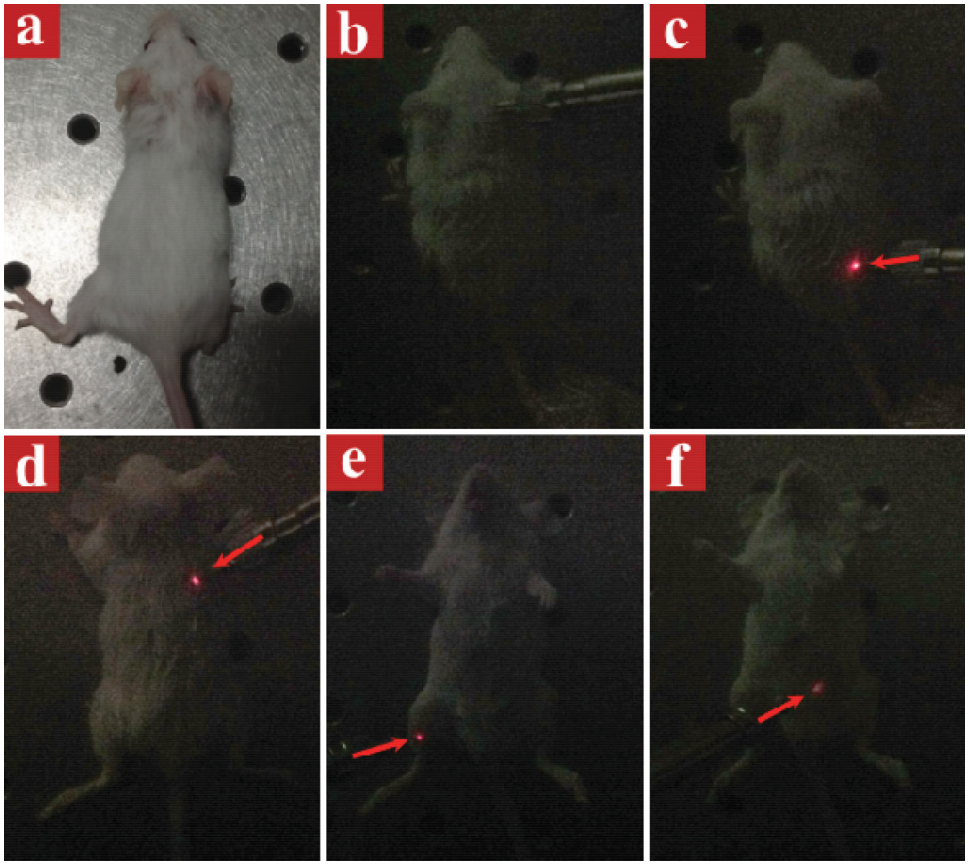

Figure 6. In vivo upconversion imaging of a Kunming mouse: (a,b) without injection of UCNPs, (c–e) with subcutaneous and (f) intraperitoneal injection of UCNPs. Note that the injected dose is 100 μL of 3 mg/mL for (c) and 100 μL of 1 mg/mL for (d–f). (b–f) Excitation under 980 nm laser.

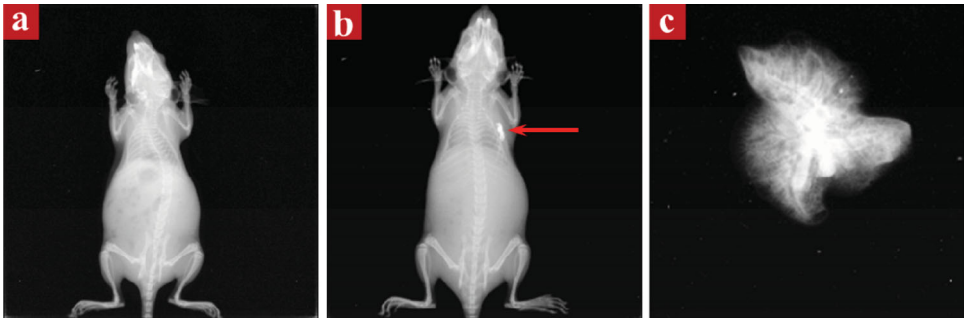

Figure 7. In vivo X-ray imaging of a nude mouse: (a) without injection of UCNPs, (b) with subcutaneous injection of UCNPs and (c) ex vivo X-ray imaging of lung, indicating visualization of blood vessel.

2.4. In Vivo Upconversion Imaging

To evaluate the UCL efficiency of these UCNPs for deeper tissue imaging, 100 µL deionized (DI) water containing different concentrations of UCNPs (3 and 1 mg/mL) was injected into different body regions of a Kunming mouse. As comparative experiments, no UCL can be observed from the mouse without treatment of UCNPs by sunlight or a 980 nm laser excitation (**Figure 6**a,b). After subcutaneous injection of UCNPs (100 µL, 3 mg/mL), obvious eye-visible red UCL was observed (labelled by red arrows as shown in Figure 6c) from the corresponding regions where the UCNPs were injected under the excitation of 980 nm laser in a dark room. Moreover, when injecting low concentration of UCNPs (100 µL, 1 mg/mL), the eye-visible red emission (Figure 6d,e) was still observed, indicating the capability of these UCNPs for deep tissue bioimaging at relatively low concentration. Figure 6f shows the bioimaging of the nude mouse with intraperitoneal injection of these UCNPs (100 µL, 1 mg/mL). As demonstrated, the red UCL is still observable by naked eyes, further indicating the red luminescence can readily penetrate to deeper location and these UCNPs are ideal probes for in vivo optical bioimaging with deep penetration and high contrast.

2.5. In Vivo X-Ray Imaging and Visualization of Blood Vessel of Lung

In addition to the dominant red UCL, these $NaLnF_4$ hosts also possess intrinsic advantages for X-ray imaging owing to the larger X-ray absorption efficiency. To verify X-ray imaging of UCNPs, in vivo and ex vivo X-ray imaging of nude mice were performed using $NaLuF_4$:Mn/Yb/Er (40/18/2 mol%) UCNPs. As shown in **Figure 7**b, the obvious X-ray signal marked by a red arrow can be observed in a nude mouse subcutaneously injected these UCNPs. More importantly, the blood vessels of lung (Figure 7c) can be readily visualized by ex vivo X-ray imaging of a scarified nude mouse after 0.5 h intravenous injection of these UCNPs. As demonstrated in our previous report,[53] no obvious signals of blood vessel were observed when untreated with UCNPs, indicating that the UCNPs can be also used as probes for blood vessels imaging, which is promising to improve the detection of pulmonary vascular diseases.

3. Conclusions

A method of transition metal Mn^{2+} doping for the simultaneous phase/size control, and multi-color output from green to red in $NaLnF_4$ (Ln = Lu, Gd, and Yb) UCNPs with fixed composition of both host and dopants of lanthanides is demonstrated. Interestingly, higher Mn^{2+} content makes larger R/G ratio in these UCNPs systems, and the significantly enhanced UCL intensity compared to Mn^{2+} free UCNPs (~59.1 times for $NaLuF_4$:Yb/Er system, ~39.3 times for $NaYbF_4$ system), and dominant red UCL make them attractive bioprobes in in vitro and in vivo bioimaging. Moreover, the in vitro cell imaging, localized UCL spectra and in vivo bioimaging reveal that these UCNPs can be applied for optical bioimaging with many advantages, such as high contrast, high signal to noise ratio, deeper tissue penetration and absence of auto-fluorescence. More importantly, the in vivo and ex vivo X-ray imaging shows these UCNPs are also multifunctional contrast agents for X-ray imaging for faster and more accurate prognosis of lung, and pulmonary vascular diseases.

4. Experimental Section

Chemicals and Materials: Rare earth (RE) nitrates $Lu(NO_3)_3$ (99.99%), $Gd(NO_3)_3$ (99.99%), $Yb(NO_3)_3$ (99.99%) and $Er(NO_3)_3$ (99.99%) were obtained from Sigma-Aldrich. Oleic acid (OA, 90%), anhydrous alcohol, $MnCl_2$ and NaF were purchased from Sinopharm Chemical Reagent Co., Shanghai, China. All other chemical reagents are of analytical grade and were used directly with no further purification.

Synthesis of $NaLnF_4$ (Ln = Lu, Gd, Yb) UCNPs: In this work, $NaLuF_4$:xMn/18Yb/2Er mol% (x = 0, 5, 10, 20, 30, and 40) UCNPs were synthesized via a modified hydrothermal process,[7,41,47] in which oleic acid was used as a capping ligand and surface modifier. At first, 0.3 g NaOH was weighed accurately and 1.5 ml DI water was added to form a clear solution. After that, 5 ml OA and 10 ml anhydrous alcohol were then added into the former mixture. A total amount of $RE(NO_3)_3$ (1 mmol) with well-designed molar ratio and NaF (4 mmol) were dropped slowly into aforementioned solution. Note that all these procedures were processed by vigorously stirring at room temperature. The homogeneous colloidal mixture was transferred into a 50 mL stainless Teflon-lined autoclave after about 20 min stirring. The system was then sealed and continuous heated at 200 °C for 8 h to favor the formation of UCNPs and growth of nanocrystals. After reaction, the system was cooled down naturally and therefore the products were obtained by washing with alcohol and DI water for several times and dried at 80 °C for 24 h. The other $NaLnF_4$-host UCNPs, such as $NaGdF_4$:Mn/Yb/Er (x/18/2 mol%) and $NaYbF_4$:Mn/Er (x/2 mol%), were prepared by using the similar method, only the corresponding $RE(NO_3)_3$ is replaced.

Synthesis of Hydrophilic Ligand-Free $NaLuF_4$:Mn/Yb/Er (40/18/2 mol%) UCNPs: In order to realize in vitro and in vivo bioimaging, the hydrophobic OA-coated $NaLuF_4$:Mn/Yb/Er were converted to the hydrophilic ligand-free $NaLuF_4$:Mn/Yb/Er by using a HCl treated method developed by Capobianco's group.[32] OA-capped $NaLuF_4$:Mn/Yb/Er (40/18/2 mol%) nanoparticles (100 mg) were added in 10 mL DI water. The aqueous mixture then reacted for 2 h by maintaining the pH value of 4 via adding HCl (0.1 M) solution. After the reaction, the carboxylate groups of the oleate ligand were yielded completely. The right amount of diethyl ether was added into the clarified solution to form two layers, namely, ether and water layers, respectively. The OA in water layer was then entirely extracted by diethyl ether for three times. The products were precipitated in acetone and then collected by centrifugation. The obtained ligand-free UCNPs were finally dispersed in water and utilized for further biological test.

Characterization: XRD patterns were recorded by a D/max-γA system X-ray diffractometer with Cu Kα radiation (λ = 1.54056 Å) at 40 kV and 250 mA. TEM, STEM, HR-TEM images, and SAED were obtained by a JEM-2100F TEM operating at 200 kV. Photoluminescence spectra were tested by a R500 spectrophotometer equipped with a 980 nm laser diode. The photographs of the as-prepared UCNPs (1 mg mL^{-1}) dispersed in cyclohexane solvent were recorded by a Canon digital camera under the excitation of a 980 nm laser (1 W cm^{-2}).

Cell Culture: HeLa cells used for in vitro imaging were cultured in Dulbecco's Modified Eagle Medium supplemented with 1% streptomycin/ penicillin and 10% fetal bovine serum at 37 °C in the atmosphere of 5% CO_2.

In Vitro Bioimaging of Ligand-Free $NaLuF_4$:Mn/Yb/Er (40/18/2 mol%) UCNPs: The as-prepared ligand-free UCNPs (100 μg mL^{-1}) were cultured with HeLa Cells at 37 °C for 24 h under the atmosphere of 5% CO_2. These HeLa cells were washed with PBS for several times and tested by a commercial confocal laser scanning microscope (ZEISS-LSM-710 NLO) equipped with a Ti: Sapphire laser (Libra II, Coherent) for in vitro bioimaging. The treated cells were detected at red region (600–700 nm) under excitation of 980 nm wavelength laser.

In Vivo Upconversion Bioimaging: 100 μL DI water containing different concentrations of UCNPs (3 and 1 mg/mL) was subcutaneously and intraperitoneally injected into different regions of a white Kunming mouse. Upconversion bioimaging was detected under the excitation of a 980 nm laser by using a digital camera (Canon). A short pass filter (800 nm) was used to eliminate the interference of the excitation light of 980 nm.

In Vivo and Ex Vivo X-Ray Bioimaging of Ligand-Free $NaLuF_4$:Mn/Yb/Er (40/18/2 mol%) UCNPs: To investigate the in vivo X-ray bioimaging of these ligand-free UCNPs, a nude mouse was anesthetized firstly by using chloral hydrate solution (10 wt%) via intraperitoneal injection. After that, the anesthetized mouse was subcutaneously injected physiological saline solutions (200 μL) containing the ligand-free $NaLuF_4$:Mn/Yb/Er (40/18/2 mol%, 3 mg/mL) UCNPs. After 0.5 h injection, the mouse was imaged by the multi-modal in vivo imaging system (Bruker In-Vivo FX PRO) equipped with an X-ray imaging accessory. The X-ray imaging was recorded under the operating voltage of 35 kVp. For ex vivo X-ray bioimaging, an other nude mouse was scarified after 0.5 h intravenous injection of these ligand-free $NaLuF_4$:Mn/Yb/Er (40/18/2 mol%, 200 μL, 3 mg/mL) UCNPs via tail vein. And the lung of the mouse was used to test the X-ray signal by the multi-modal in vivo imaging system. A high resolution X-ray imaging of the blood vessel of the lung was captured under the operating voltage of 35 kVp with 3.3X geometric magnification stage.

Supporting Information

Supporting Information is available from the Wiley Online Library or from the author.

Acknowledgements

This work was supported by the National Natural Science Foundation of China (Nos. 51102202, and 31370736), Specialized Research Fund for the Doctoral Program of Higher Education of China (No. 20114301120006) and Program for new Century Excellent Talents in University (NCET-13–0787), and Hunan Provincial Natural Science Foundation of China (Nos. 12JJ4056 and 13JJ1017), and the Scientific Foundation of Ministry of Education (212119) and Scientific Research Fund of Hunan Provincial Education Department (13B062), and the Fundamental Research Funds for the Central Universities(WK2070000007). We thank Prof. Guoqiang Bi, and Dr. Xiaokang Zhang in University of Science and Technology of China for in vitro cell imaging and helpful discussions.

Received: December 23, 2013
Revised: January 25, 2014
Published online: March 24, 2014

[1] G. Y. Chen, T. Y. Ohulchanskyy, R. Kumar, H. Ågren, P. N. Prasad, *ACS Nano* **2010**, *4*, 3163.
[2] M. Haase, H. Schäfer, *Angew. Chem., Int. Ed.* **2011**, *50*, 5808.
[3] F. Wang, X. G. Liu, *Chem. Soc. Rev.* **2009**, *38*, 976.
[4] J. Zhou, Z. Liu, F. Y. Li, *Chem. Soc. Rev.* **2012**, *41*, 1323.
[5] S. Sivakumar, F. C. J. M. van Veggel, M. Raudsepp, *J. Am. Chem. Soc.* **2005**, *127*, 12464.
[6] Y. S. Liu, D. T. Tu, H. M. Zhu, X. Y. Chen, *Chem. Soc. Rev.* **2013**, *42*, 6924.
[7] X. Wang, J. Zhuang, Q. Peng, Y. D. Li, *Nature* **2005**, *437*, 121.
[8] F. Wang, Y. Han, C. S. Lim, Y. H. Lu, J. Wang, J. Xu, H. Y. Chen, C. Zhang, M. H. Hong, X. G. Liu, *Nature* **2010**, *463*, 1061.
[9] N. M. Idris, M. K. Gnanasammandhan, J. Zhang, P. C. Ho, R. Mahendran, Y. Zhang, *Nature Medicine* **2012**, *18*, 1580.
[10] M. Nyk, R. Kumar, T. Y. Ohulchanskyy, E. J. Bergey, P. N. Prasad, *Nano Lett.* **2008**, *8*, 3834.
[11] S. L. Gai, P. P. Yang, C. X. Li, W. X. Wang, Y. L. Dai, N. Niu, J. Lin, *Adv. Funct. Mater.* **2010**, *20*, 1166.
[12] W. P. Fan, B. Shen, W. B. Bu, F. Chen, K. L. Zhao, S. J. Zhang, L. P. Zhou, W. J. Peng, Q. F. Xiao, H. Y. Xing, J. N. Liu, D. L. Ni, Q. J. He, J. L. Shi, *J. Am. Chem. Soc.* **2013**, *135*, 6494.
[13] Y. L. Dai, P. A. Ma, Z. Y. Cheng, X. J. Kang, X. Zhang, Z. Y. Hou, C. X. Li, D. M. Yang, X. F. Zhai, J. Lin, *ACS Nano* **2012**, *6*, 3327.
[14] F. Wang, R. R. Deng, J. Wang, Q. X. Wang, Y. Han, H. M. Zhu, X. Y. Chen, X. G. Liu, *Nature Mater.* **2011**, *10*, 968.
[15] J. Zhou, X. Zhu, M. Chen, Y. Sun, F. Y. Li, *Biomaterials* **2012**, *33*, 6201.
[16] C. X. Li, Z. Y. Hou, Y. L. Dai, D. M. Yang, Z. Y. Cheng, P. A. Ma, J. Lin, *Biomater. Sci.* **2013**, *1*, 213.
[17] H. Schäfer, P. Ptacek, H. Eickmeier, M. Haase, *Adv. Funct. Mater.* **2009**, *19*, 3091.
[18] N. Niu, P. P. Yang, F. He, X. Zhang, S. L. Gai, C. X. Li, J. Lin, *J. Mater. Chem.* **2012**, *22*, 10889.
[19] U. Rocha, C. J. da Silva, W. F. Silva, I. Guedes, A. Benayas, L. M. Maestro, M. A. Elias, E. Bovero, F. C. J. M. van Veggel, J. A. G. Solé, D. Jaque, *ACS Nano* **2013**, *7*, 1188.
[20] H. S. Qian, H. C. Guo, P. C. L. Ho, R. Mahendran, Y. Zhang, *Small* **2009**, *5*, 2285.
[21] J. C. Boyer, F. Vetrone, L. A. Cuccia, J. A. Capobianco, *J. Am. Chem. Soc.* **2006**, *128*, 7444.
[22] Y. F. Wang, G. Y. Liu, L. D. Sun, J. W. Xiao, J. C. Zhou, C. H. Yan, *ACS Nano* **2013**, *7*, 7200.
[23] X. Teng, Y. H. Zhu, W. Wei, S. C. Wang, J. F. Huang, R. Naccache, W. B. Hu, A. I. Y. Tok, Y. Han, Q. C. Zhang, Q. L. Fan, W. Huang, J. A. Capobianco, L. Huang, *J. Am. Chem. Soc.* **2012**, *134*, 8340.
[24] F. Chen, W. B. Bu, S. J. Zhang, J. N. Liu, W. P. Fan, L. P. Zhou, W. J. Peng, J. L. Shi, *Adv. Funct. Mater.* **2013**, *23*, 298.
[25] L. Cheng, K. Yang, Y. G. Li, X. Zeng, M. W. Shao, S. T. Lee, Z. Liu, *Biomaterials* **2012**, *33*, 2215.
[26] Q. Liu, Y. Sun, T. S. Yang, W. Feng, C. G. Li, F. Y. Li, *J. Am. Chem. Soc.* **2011**, *133*, 17122.

[27] F. Zhang, D. Y. Zhao, *ACS Nano* **2009**, *3*, 159.
[28] S. L. Gai, C. X. Li, P. P. Yang, J. Lin, *Chem. Rev.* **2013**, DOI: 10.1021/cr4001594.
[29] C. Wang, H. Q. Tao, L. Cheng, Z. Liu, *Biomaterials* **2011**, *32*, 6145.
[30] S. J. Zeng, M. K. Tsang, C. F. Chan, K. L. Wong, J. H. Hao, *Biomaterials* **2012**, *33*, 9232.
[31] H. R. Liu, W. Lu, H. B. Wang, L. Rao, Z. G. Yi, S. J. Zeng, J. H. Hao, *Nanoscale* **2013**, *5*, 6023.
[32] N. Bogdan, F. Vetrone, G. A. Ozin, J. A. Capobianco, *Nano Lett.* **2011**, *11*, 835.
[33] D. Q. Chen, P. Huang, Y. L. Yu, F. Huang, A. P. Yang, Y. S. Wang, *Chem. Commun.* **2011**, *47*, 5801.
[34] J. C. Boyer, F. C. J. M. van Veggel, *Nanoscale* **2012**, *2*, 1417.
[35] C. Li, J. Lin, *J. Mater. Chem.* **2010**, *20*, 6831.
[36] Q. F. Xiao, X. P. Zheng, W. B. Bu, W. Q. Ge, S. J. Zhang, F. Chen, H. Y. Xing, Q. G. Ren, W. P. Fan, K. L. Zhao, Y. Q. Hua, J. L. Shi, *J. Am. Chem. Soc.* **2013**, *135*, 13041.
[37] X. J. Xie, N. Y. Gao, R. R. Deng, Q. Sun, Q. H. Xu, X. G. Liu, *J. Am. Chem. Soc.* **2013**, *135*, 12608.
[38] S. J. Zeng, M. K. Tsang, C. F. Chan, K. L. Wong, B. Fei, J. H. Hao, *Nanoscale* **2012**, *4*, 5118.
[39] J. B. Zhao, D. Y. Jin, E. P. Schartner, Y. Q. Lu, Y. J. Liu, A. V. Zvyagin, L. X. Zhang, J. M. Dawes, P. Xi, J. A. Piper, E. M. Goldys, T. M. Monro, *Nature Nanotechnol.* **2013**, *8*, 729.
[40] J. Wang, F. Wang, C. Wang, Z. Liu, X. G. Liu, *Angew. Chem., Int. Ed.* **2011**, *50*, 10369.
[41] G. Tian, Z. J. Gu, L. J. Zhou, W. Y. Yin, X. X. Liu, L. Yan, S. Jin, W. L. Ren, G. M. Xing, S. J. Li, Y. L. Zhao, *Adv. Mater.* **2012**, *24*, 1226.
[42] H. Kobayashi, M. Ogawa, R. Alford, P. L. Choyke, Y. Urano, *Chem. Rev.* **2010**, *110*, 2620.
[43] J. H. Hao, Y. Zhang, X. H. Wei, *Angew. Chem. Int. Ed.* **2011**, *50*, 6876.
[44] Y. L. Liu, K. L. Ai, J. H. Liu, Q. H. Yuan, Y. Y. He, L. H. Lu, *Angew. Chem. Int. Ed.* **2012**, *51*, 1437.
[45] S. B. Yu, A. D. Watson, *Chem. Rev.* **1999**, *99*, 2353.
[46] http://physics.nist.gov/PhysRefData/XrayMassCoef/, accessed: October, 2013.
[47] S. J. Zeng, J. J. Xiao, Q. B. Yang, J. H. Hao, *J. Mater. Chem.* **2012**, *22*, 9870.
[48] R. D. Shannon, *Acta Cryst.* **1976**, *A32*, 751.
[49] D. Q. Chen, Y. L. Yu, F. Huang, P. Huang, A. P. Yang, Y. S. Wang, *J. Am. Chem. Soc.* **2010**, *132*, 9976.
[50] F. Vetrone, J. C. Boyer, J. A. Capobianco, A. Speghini, M. Bettinelli, *J. Appl. Phys.* **2004**, *96*, 661.
[51] S. J. Zeng, G. Z. Ren, Q. B. Yang, *J. Mater. Chem.* **2010**, *20*, 2152.
[52] X. Y. Li, H. J. Liu, X. X. Sun, G. Q. Bi, G. Q. Zhang, *Adv. Optical Mater.* **2013**, *1*, 549.
[53] S. J. Zeng, H. B. Wang, W. Lu, Z. G. Yi, L. Rao, H. R. Liu, J. H. Hao, *Biomaterials* **2014**, *35*, 2934.